Stony Brook University

OFFICIAL COPY

The official electronic file of this thesis or dissertation is maintained by the University Libraries on behalf of The Graduate School at Stony Brook University.

© All Rights Reserved by Author.

Plasmonic nanoclusters based on conjugated polymer for controlled optical output

A Thesis presented

by

Xuyi Wang

to

The Graduate School

In Partial Fulfillment of the

Requirements

For the Degree of

Masters of Science

in

Materials Sciences and Engineering

Stony Brook University

May 2013

Copyright by

Xuyi Wang

2013

Stony Brook University
The Graduate School

Xuyi Wang

We, the thesis committee for the above candidate for the

Master of Science degree, hereby recommend

Acceptance of the thesis

Dr. Mircea Cotlet, Professor, Materials Sciences & Engineering

Dr. Gersappe, Professor, Materials Sciences & Engineering

Dr. Venkatesh, Assistant Professor, Materials Sciences & Engineering

This thesis is accepted by the Graduate School

Charles Taber

Interim Dean of the Graduate School

Abstract of the thesis

Conjugated polymer based plasmonic nanoclusters with controlled optical output

by

Xuyi Wang

Master of Science

In

Masterials Sciences and Engineering

Stony Brook University

2013

Rational design and assembly of colloidal metal nanoparticles with fluorescent materials like organic dyes, conjugated polymers or colloidal quantum dots has stimulated intense research interest in the past decade in view of obtaining nanomaterials with controllable optical properties and with applicability in optoelectronics and biosensing. The interaction between a fluorescent molecule and a metal nanoparticle, also known as plasmon-exciton interaction, is determined by several factors such as type, shape and size of the metal nanoparticle, electronic properties of the fluorescent molecule, metal nanoparticle-fluorescence molecule separation distance and local nanoenvironment. By tuning one or more of such factors one can achieve control of the plasmon-exciton interaction and therefore of the optical output. This research reports assembly by electrostatic binding and the single particle characterization of a series of plasmonic nanoclusters based on core/shell Au/SiO_2 nanoparticle capped with a water soluble conjugated polythiophene derivative. By

varying the thickness of the SiO_2 spacer we demonstrate the ability to control the photoluminescence output of the metal nanoparticle/conjugated polymer nanocluster. Plasmonic nanoclusters exhibiting enhanced photoluminensce were further conjugated with Cytochrome C to investigate plasmon-assisted photoinduced charge transfer from the polymer to Cytochrome C.

ACKNOWLEDGMENTS

First and foremost, I would like to thank my advisor, Dr. Mircea Cotlet for his constant encouragement and guidance throughout my Master. I am truly grateful for your support through the ups and downs.

I also would like to also thank Mr. Zhongwei Liu for his tireless efforts in helping me achieve my goals. Thanks for sharing your bench and your wealth of knowledge so patiently.

I would also like to thank Dr. Zhihua Xu for all his help and guide on how to efficiently do my experiment over the past year. Your theoretical models and patience at trying to explain them to me were truly appreciated. I learnt an incredible amount from you. Thanks for your time and patience.

I would also like to thank all the members of the bio-soft nanomaterials group at CFN in Brookhaven National Lab, both past and present. Thank you for your support and creating a wonderful place to come in to every day, which help make my time at CFN so productive and pleasurable.

The research reported herein was carried out in whole at the Center for Functional Nanomaterials, Brookhaven National Laboratory, which is supported by the U.S. Department of Energy, Office of Basic Energy Sciences, under Contract No. DE-AC02-98CH10886.

TABLE OF CONTENTS

LIST OF FIGURES

CHAPTER 1. INTRODUCTION

1.1 Background

Noble metal nanostructures are known to exhibit remarkable and synthetically taylorable plasmonic properties owing to their surface plasmon modes. Surface plasmons are defined as collective electron oscillations in metallic nanoparticles that are excited by light[1]. When the frequency of photons matches the oscillation frequency of the "free" electrons on a metallic surface, the surface plasmon resonance is achieved[2]. The interaction between such surface plasmons and nearby fluorescent molecules can influence the molecule electronic properties, modulating the fluorescence response of the molecule[3]. This plasmon-exciton interaction has been the subject of many research reports and applied to the development of various nanomaterials in optoelectronics and biosensing[4],[5],[6].

For optoelectronic applications, metal nanostructures such as nanoparticles, nanoprisms, nanorods, nanogratings, etc. have been incorporated in both photovoltaic solar cells and light emitting diodes to enhance the performance of such devices [7], [8]. For example, when gold nanoshells are embedded into the quantum dot absorber film layer in a solar cell, it can help efficiently control and enhance propagation and absorption of incoming light, with some solar cells achieving a 35% enhancement in photocurrent[9].

Plasmon nanomaterials have been used also in the development of biosensors in particular for enhancing sensitivity in detection in electrochemical and fluorescence-based assays[10]. For example, when fluorescently-labeled biomolecules such as proteins or DNA are additionally labeled with gold nanoparticles, a stronger photoluminescence signal can be attained providing increased detection sensitivity [11].

1.2 Fundamental aspects of plasmon– exciton interactions

Light illuminating a metal nanostructure can excite localized surface plasmon resonances so that if a fluorescent molecule is localized nearby it can impact its electronic properties in several ways. It can enhance the molecular excitation rate by increasing the local electric field, it can quench the fluorescence by introducing competing nonradiative channels such as nonradiative energy transfer or it can increase the fluorescence rate when the plasmon and fluorescence are in resonance[12], [13]. It is easy to understand the plasmon-exciton interaction by modeling the fluorescent emitted by the molecule as a two-state process, a first one involving excitation and a second one involving emission of fluorescence. In the excitation process, the rate for excitation is influenced by the local electric field by the Fermi's golden rule,

$$k_{exc} = (\frac{4\pi^2}{h})|\langle e|\boldsymbol{E}\cdot\boldsymbol{p}|g\rangle|^2\rho_e \qquad (1.1)$$

Where h is Plank constant, e and g are wave functions for the excited and ground state, $\boldsymbol{E}$ is the local electric field, $\boldsymbol{p}$ is the dipole moment of the molecule and ρ_e is the density of the excited state[14]. In the emission process, this step is regulated by the quantum yield of fluorescence according to

$$\phi = \frac{k_r}{k_r+k_{nr}} \qquad (1.2)$$

Where k_r, k_{nr}, are rates for radiative deactivation (spontaneous emission) and nonradiative deactivation. The fluorescence emission intensity is given by

$$I = k_{exc} \times \phi \qquad (1.3)$$

When a plasmonic nanoparticle is present in the proximity of the fluorescent molecule, the emission intensity can vary in two ways. The excitation rate can be increased by the local electric field enhancement which can be due to the optical excitation of

localized surface plasmon resonances in the metal nanoparticle and according to eq.1.1 and eq.1.3 this will increase the intensity of fluorescence. Once in the excited state, the fluorescent molecule (exciton) can decay by three pathways: (i) radiative decay by the emission of a photon, (ii) nonradiative decay through its internal channels and (iii) by energy transfer to the metal nanoparticle where it excites the localized plasmon resonance of the metal. The coupling of the plasmon with the exciton can affect both radiative and nonradiative rates k_r and k_{nr}. The excited localized plasmon can decay radiative thus emitting a photon or nonradiative, resulting in quenching of fluorescence. The balance between nonradiative and radiative decay for the localized plasmon is a relationship between the absorption and scattering cross section of the metal nanoparticle at the emission wavelength of the fluorescent molecule[15]. For coupled localized plasmon resonance and exciton having surface plasmon resonance band and fluorescence emission band in strong overlap, the radiative rate can be enhanced and this results in the increase in intensity[16]. For uncoupled resonance or no spectral overlap, the nonradiative rate for energy transfer is enhanced and this results in quenching. For these plasmonic nanosystems, an overall enhancement results from the competing enhancement by excitation rate over nonradiative energy transfer to metal nanoparticle. Non-radiative energy transfer rate depends on the separation distance between the fluorescent molecule and the metal nanoparticle while the local field enhancement can be biased by the type, size and shape of the metal nanoparticle[17]. Therefore, an easy way to control the intensity of emitted fluorescence is to vary the separation distance, for example by using an optical inert material or the size of the metal nanoparticle.

1.2.1 Metal nanoparticle size and distance effects on plasmon-exciton interactions

The metal NP's size has an important effect on the surface plasmon resonance (SPR) band[18]. Generally, for the gold nanoparticles (diameter greater than approximately 10nm), as the particle size increases, the peak of SPR shifts to longer wavelengths[19]. Fig. 1.1 shows the SPR vs size for gold spherical nanoparticles. If the particle size continues to increase toward the bulk, the SPR moves into infrared and most of the visible light is reflected. By changing the size of the nanoparticle, one can overlap the plasmon resonance with the fluorescence band of a given molecule and therefore enhance the radiative rate or it can simply enhance the excitation rate when using larger size nanoparticles to obtain an enhancement in the local electric field.

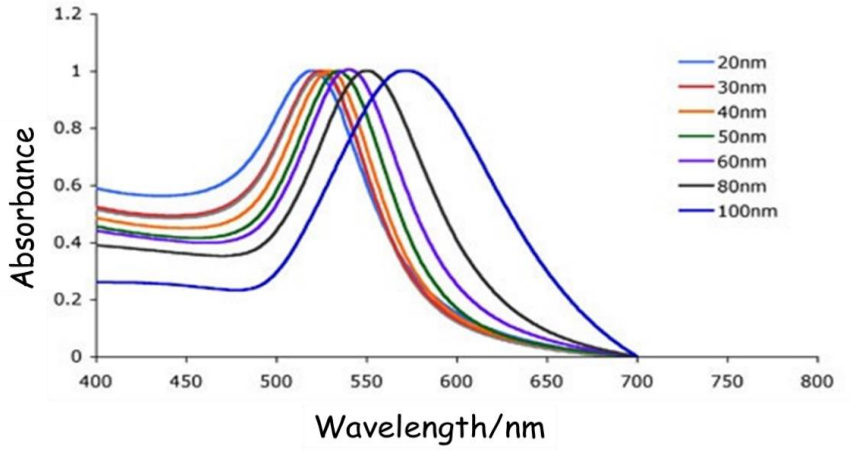

Figure 1. 1: Plasmon band spectrum of gold nanoparticles which size increases from 20nm to 100nm.

The separation distance between the fluorescent molecule and metal nanoparticle (NP) and the color (wavelength) of incoming light are both have important effects on the plasmon-exciton interaction, as they can control the competition between nonradiative energy transfer to the metal and plasmon enhancement by local electric field (excitation rate)[20]. Fig. 1.2 shows theoretical calculations for the expected fluorescence enhancement as a function of intercomponent distance and wavelength of excitation

for a fluorescent molecule emitting at 600nm in the vicinity of a 60nm size gold nanoparticle according to reference[21] . According to Figure 1.2, if the intercomponent distance is less than 10nm, the fluorescence of the emitter will be quenched as at short distances the plasmon-exciton interaction is dominated by non-radiative energy transfer[22]. If the distance is larger than 15nm, the fluorescence of emitter will be enhanced by the plasmon effect, mainly increase in the excitation rate as plasmon resonance (530nm) and fluorescence (600nm) do not overlap. Some recent reports showed that it is possible to control the optical output of a plasmonic nanocluster composed of a gold NP and a colloidal quantum dot by the use of DNA linkers. The results shows when the DNA linker (intercomponent) is around 30nm, the fluorescence of quantum dots can be enhanced around 5 times[23].

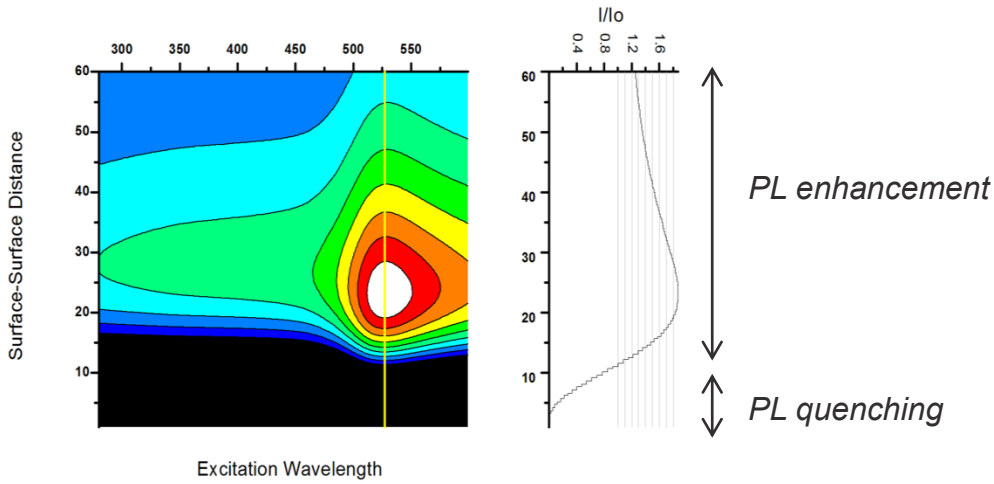

Figure 1. 2: PL enhancement vs. Surface-surface and excitation wavelength. Unpublished results provided by M.Sfeir from Brookhaven National Laboratory, New York.

1.3 Self-assembly methods

Self- assembly of molecules can be realized through non-covalent interactions (e.g., hydrogen bonding, metal coordination, hydrophobic forces, van der Waals forces, π-π interactions, and/or electrostatic)[24], [25], [26]. Some important examples of self-assembly in materials science involve the formation of molecular crystals, DNA self-recognition, antibody-antigen interactions, phase-separated polymers, and self-assembled monolayers by electrostatic interactions (layer-by-layer) [27]. The following will specifically introduce some recent studying method for self-assembly.

1.3.1 Self-Assembly Based on biomolecular self-recognition

DNA has unique molecular recognition properties and it can combine other nucleic acids to create self-assembling branched DNA complexes with useful properties. Recently, many nano-structures have been built by utilizing this self-recognition ability of DNA. For example, some nanoparticles encoded with DNA can be recognized into nanoaggregates by DNA base pair self-assembly method[28]. Fig. 1.3 shows heterodimers assembly, which were composed of a colloidal quantum dot and a gold nanoparticle linked via dsDNA. They were prepared via a step-wise surface-based DNA self-assembly method with dimeric stoichiometry and varying interparticle distance given by the length of the DNA linker connecting the two nanoparticles. Among these dimers, those with a DNA-defined interparticle distance of ~30 nm can achieve photoluminescence enhancement from gold plasmon effect, on average 5 times[23].

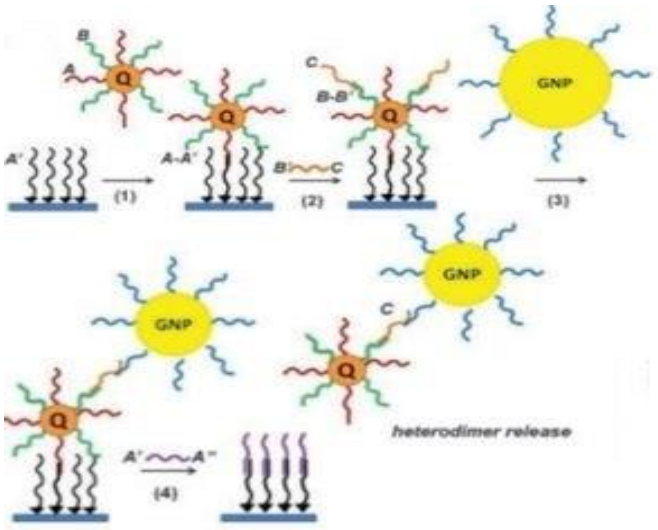

Figure 1. 3: Surface-based approach for the assembly of Qdot–AuNP heterodimers. Q, Qdot; GNP, AuNP. Reproduced from reference[23]

In addition, antibody-antigen recognition is another common molecular self-assembly method. Biosensing platforms have been proposed in which biomolecules can be detected by combining them with metal nanoparticles via antibody-antigen self-recognition[29].

1.3.2 Layer-by-layer (LbL) method

Layer-by-layer (LBL) assembly is a simple, versatile, and significantly inexpensive approach by which nanocomponents of different groups can be combined to coat both macroscopically flat and non-planar (e.g., colloidal core-shell particles) surfaces[30]. It also has been widely used for plasmonic biology detection. In LbL assembly, we can employed its molecular spacers to tune the vertical separation of fluorophore from the metal (Au or Ag) surface, which help precisely modulate plasmon-exciton interactions and the photoluminescence (PL) of fluorophore[31].

CHAPTER 2. Materials and Methods

2.1 Materials

2.1.1 Conjugated Polymer-PHT

Poly [2-(3-thienyl) ethyloxy-4-butylsulfonate] sodium salt (PHT) was obtained from QCR Solutions Corp (Port St. Lucie, FL) as a water soluble conjugated polymer with negative charges due to sulfonate functional group. The chemical structure is shown in Fig. 2.1. Since this conjugated polythiophene polymer has extended π-systems backbone, it has some unique delocalized electronic and optical properties. Absorption and Emission Spectrum of polymer PHT (pH 7) are shown in Fig. 2.1. The peaks for absorption and emission are around 410nm and 580nm, respectively, and it emits with a quantum yield of 5%. In addition, optical properties of PHT solution has a dependence on the pH. Increasing alkaline pH in solution leads to the more charged side chains for PHT, which causes a more planar conformation of the backbone and aggregation of the polymer chains, and the PHT spectra will be shifted toward red.

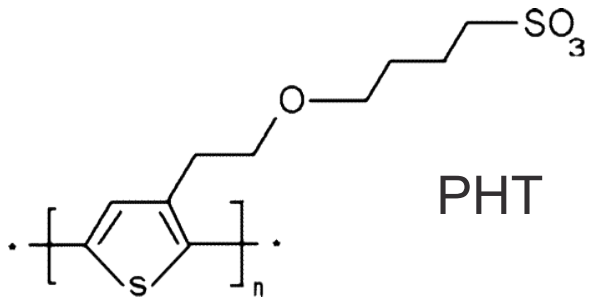

Figure 2. 1: Chemical structure of Poly [2-(3-thienyl) ethyloxy-4-butylsulfonate] sodium salt

2.1.2 Gold-silica core-shell nanoparticles (AuNP/SiO_2)

Au/SiO2 core/shell nanoparticle are usually synthesized by well-established solgel chemistry methods such as the Strober method by starting with commercially available metal (Au, Ag) NPs[32]. The surface of silica shell can be modified with functional amino group to become positively charged (Figure 2.2). We used four different types of core/shell Au/SiO2, each with a 50nm gold core and various shell thicknesses, 10, 16, 19 and 30nm custom made by Nanocomposix (San Diego, CA). Some physical parameters are shown in table 1.

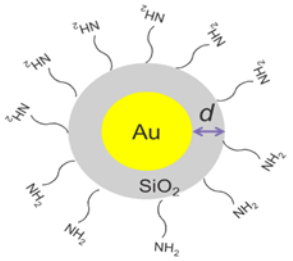

Figure 2. 2: Sketch of Silica Coated 50nm Gold Nanospheres

Table 1: Physical parameters of Au/SiO_2 core/shell nanoparticle

Silica shell thickness (50nm core Au)	plasmon band peak	Hydrodynamic Diameter
10nm	537nm	133.8nm
16mn	535nm	102.1nm
19nm	534nm	107.4nm
30nm	543nm	130.9nm

2.1.3 Self-assembly for Au/SiO_2 and PHT

We assembled PHT and Au/SiO_2 by electrostatic binding in water (pH 7) with PHT coating the surface of positively charged Au/SiO_2, thus forming a Au/SIO_2-PHT complex (Fig. 2.3) with the polymer and AuNP separated by the SiO_2 shell which varies among the four samples to investigate the plasmon-assisted photoluminescence of the conjugated PHT.

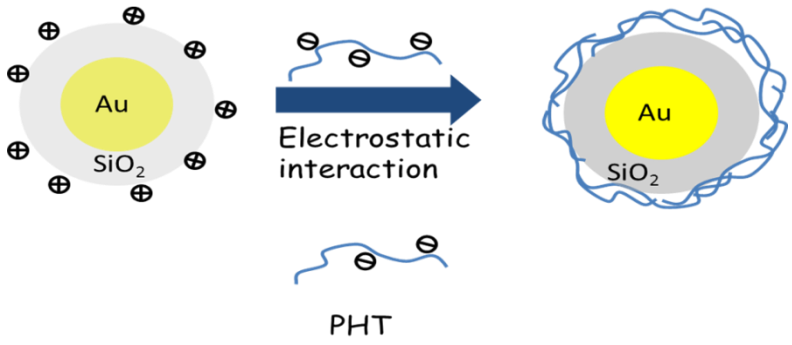

Figure 2. 3: Schematic of So Au/SIO2 –PHT composites

2.1.4 Cytochrome C

Cytochrome C is a small heme protein which is part of the electron transport chain in mitochondria, accepting one electron. Cytochrome C is highly soluble in water, it has a high isoelectric point (10) which means it is positively charged at neutral pH and can be assembled on the AuSiO2-PHT plasmonic nanocluster at the outer silica shell to form a plasmonic donor-acceptor charge transfer nanocluster. Fig. 2.4 shows the absorption spectrum of cytochrome C with the main peak around 405nm. In Fig. 2.5 the energy difference between the lowest unoccupied molecular orbit (LUMO) of the conjugated polymer (donor) and protein (acceptor) ensures efficient electron transfer from polymer PHT to Cytochrome C. For the presented experiments, cytochrome c from bovine heart was obtained from Sigma-Aldrich as poweder (St. Louis, MO).

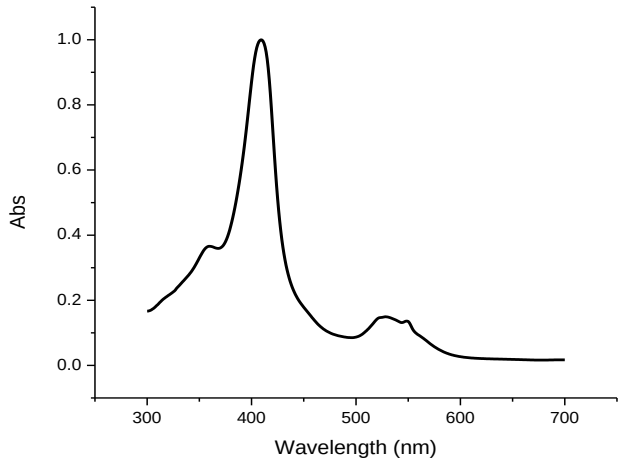

Figure 2. 4: Normalized Absorption spectrum of Cytochrome C

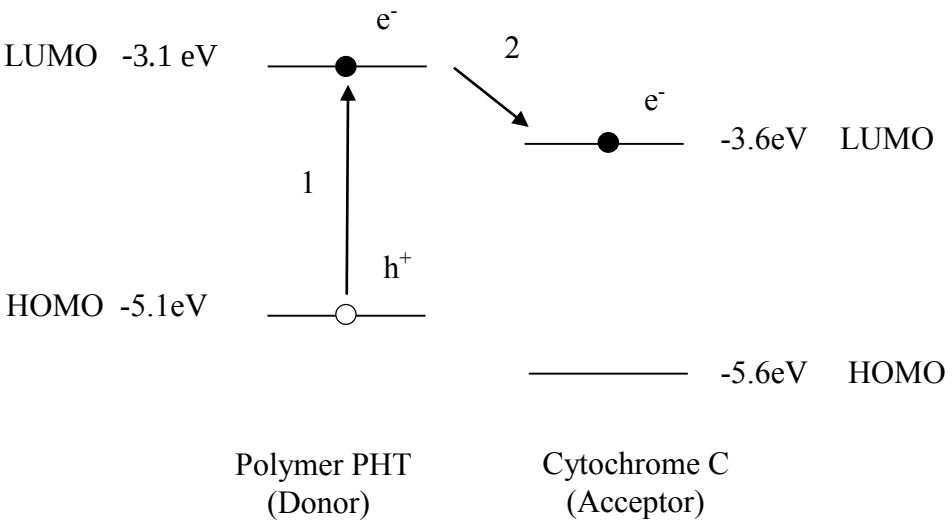

Figure 2. 5: A difference in energy level between polymer PHT donor and Cytochrome C acceptor is essential for efficient exciton creation (1) and electron transfer (2). LUMO: Lowest unoccupied molecular orbit. HOMO: Highest occupied molecular orbit.

2.2 DLS for confirming particle formation and non-aggregation

Dynamic light scattering (DLS) is usually used to measure the size and size distribution of molecules and nanoparticles typically in the submicron region[33]. The basic principle of the method consists of shining a laser beam through a solution containing diluted nanoparticles. The Brownian motion of these particles in solution causes the laser light to be scattered at different angle intensities[34]. Experimentally one characterizes these intensity fluctuations of the scattered light by computing the second order correlation function of the intensity, whose analysis by a three-dimensional diffusion model can provide the diffusion coefficient of the particles. The Stokes Einstein formula (shown in equation 2.1) can be used to calculate the hydrodynamic radius Rh of the particles in solution.

$$R_h = \frac{k_B T}{6\pi\eta D} \qquad (2.1)$$

Where R= hydrodynamic radius, k_B is the Boltzmann constant, T the temperature, and η the shear viscosity of the solvent, D = Diffusion co-efficient[35]. In our case, the method is used to prove successful assembly of $AuSiO_2$-PHT nanocomposites and the lack of aggregation of the assembled nanocomposites. The experiments were performed on a Malvern-Zetasizer DLS instrument with a 632nm He Ne laser.

2.3 Single particle photoluminescence microscopy

Single molecule optical microscopy (SMS) has evolved in the past two decades as an important tool to investigate processes in many areas, from biology, to chemistry to physics[36]. Compared to the traditional ensemble spectroscopy which can only measure average properties, single molecule spectroscopy interrogates one molecule at a time

and as such it removes ensemble averaging, resolves heterogeneity and subpopulation of molecules behaving different and it can capture transient species that might not be detectable in ensemble due to their low contribution[37]. For plasmon-assisted fluorescence studies, single molecule microscopy has a large advantage over conventional photoluminescence spectroscopy by using narrow laser lines for excitation and optical filters for rejection of scattering, thus measuring the real plasmon-assisted fluorescence signal[23]. Confocal-based single molecule fluorescence microscopy with time-resolved detection by the time-correlated single photon counting (TCSPC) method allows measurement of several molecular parameters simultaneously, for example fluorescence intensity, lifetime, and fluorescence spectrum on a molecule by molecule basis. In TCSPC one records the time dependent intensity profile of the emitted fluorescence (decay curve) upon excitation by a short flash of light, typically a laser pulse[38]. TCSPC measures the arrival time of the emitted photons with respect to the laser pulse and photons from multiple excitation/emission cycles to retrieve the lifetime of a fluorescent molecule or the decay times associated with different processes present in the molecule. In single molecule microscopy, TCSPC can be implemented in a time-tagged time-resolved mode as shown in Fig 2.6 by recording for each photon from a single molecule both the arrival time with respect to the laser pulse (microtime) and with respect to the beginning of the experiment (macrotime)[39]. The microtime information is histogrammed to build fluorescence decay curves and the macrotime to build time traces of fluorescence intensity. If the single molecules to be probed are immobilized on a substrate, a scanning method can be implemented to obtain fluorescence lifetime imaging microscopy (FLIM) with single molecule sensitivity[40].

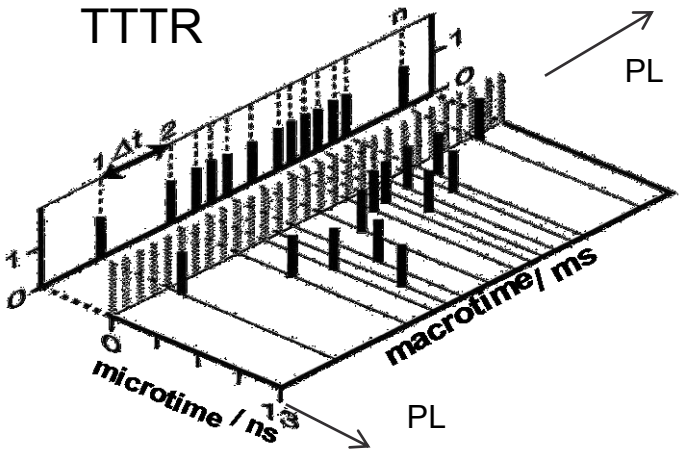

Figure 2. 6: Time-Tagged Time-Resolved SMS[41]

2.3.3 Experimental setup for fluorescence decay measurements with TCSPC

Single molecule fluorescence experiments were performed with an Olympus IX81 inverted confocal microscope equipped with a 1.4 NA oil immersion lens and coupled to a picosecond solid-state diode laser featuring 440 nm and 532nm laser light at 10 MHz). The schematics of the microscope is shown in Fig.2.7. The microscope was equipped with a piezo-scanner for imaging via FLIM Fluorescence was collected by the same lens, spectrally separated from excitation laser by a dichroic mirror (R532, Semrock Filters) imaged onto a 75 μm pinhole and then split by a 50/50 beam splitter onto two single photon counting avalanche photo diode detectors (MPD, Picoquant GmbH, Germany). One detector was used to image the backscattering signal from the gold nanoparticles by using a narrow bandpass filter centered on the laser light (Semrock, 532/3 bandpass) while the second detector imaged the fluorescence from the polymer PHT with a 650nm/50 bandpass filter (Semrock). Signals from both detectors were fed onto a time analyzer (PicoHarp300) and recorded by a commercial software, Symphotime (Picoquant GmbH, Germany).

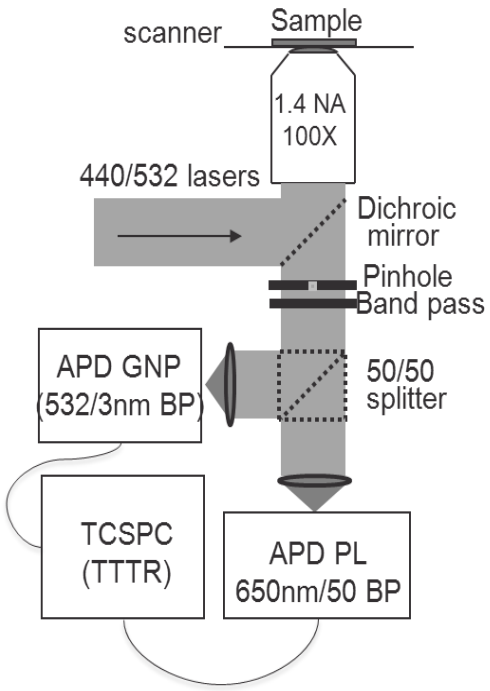

Figure 2. 7: Schematic of single molecule microscopy

CHAPTER 3. Results and Discussion

3.1 UV-VIS AND PHOTOLUMINESCENCE SPECTROSCOPY

Fig. 3.1 shows the UV-vis spectrum of the 50 nm Au/SiO2 NPs (19 nm shell thickness) in water and the UV-vis and photoluminescence (PL) spectra of conjugated PHT in water. The surface plasmon resonance (SPR) peak from Au/SiO2 NPs for various shell thicknesses between 10nm and 30nm peaks in the range 537-543nm (see table 1), slightly red shifted comapred to bare 50nm goldnanoparticles (SPR at around 530nm). For PHT, the absorption peak is located at 410nm and extends broadly onto low energy part of the visible spectrum, up to 600nm while the PL peaks at 580nm and overalps considerably with the SPR of the AuNP/SiO2. to ensure plasmon-exciton interaction in a AuNP/SiO2-PHT nanocomposite. For example, these nanocomposites can be excited at 440nm and considered off-SPR, and at SPR with 532nm to monitor and quantify changes in PL intensity and lifetime as a function of shell thickness which here will dictate the separation distance between the plasmonic and excitonic components.

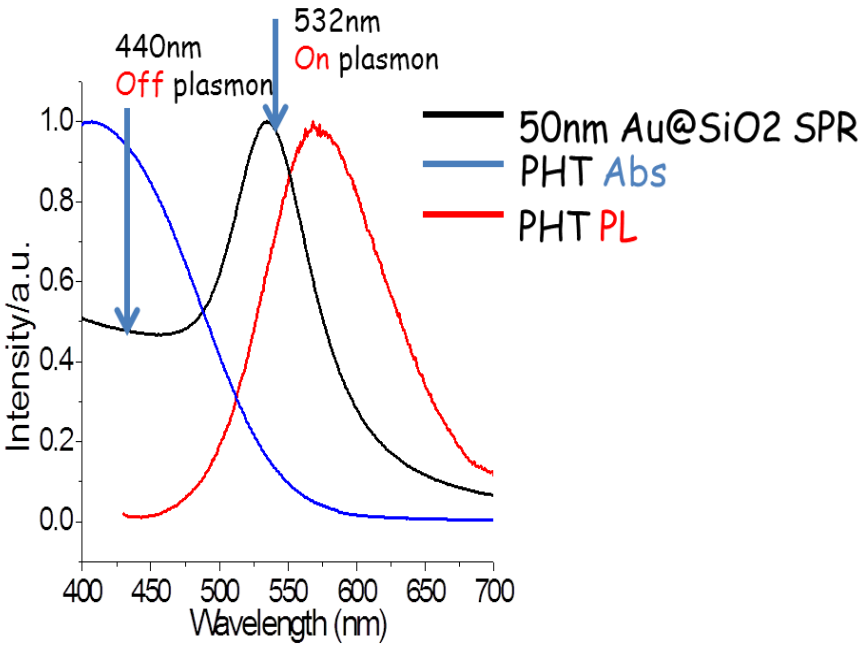

Figure 3. 1: UV-vis spectrum of 50 nm Au/SiO2 NPs in water (black line). UV-vis and PL spectra (440 nm excitation) of PHT in water.

3.2 Dynamic Light Scattering of Au/SiO_2-PHT nanocomposites

Size distribution of Au/SiO_2 nanoparticles and Au/SiO_2-PHT composites were determined by dynamic light scattering (DLS) to demonstrate electrostatic binding of PHT to the aminated surface of AuNP/SiO2 and at the same time to prove that there is no aggregation of the formed nanocomposites. The size distribution for the four types of nanocomposites is shown in Fig. 3.2 and for all of them we observed an increase in particle size from Au/SiO_2 nanoparticles to Au/SiO_2 –PHT nononomposites. The observed variation in particle size, Δd is in the range 4-10nm and this variation might be attributed to the errors from the DLS estimation.

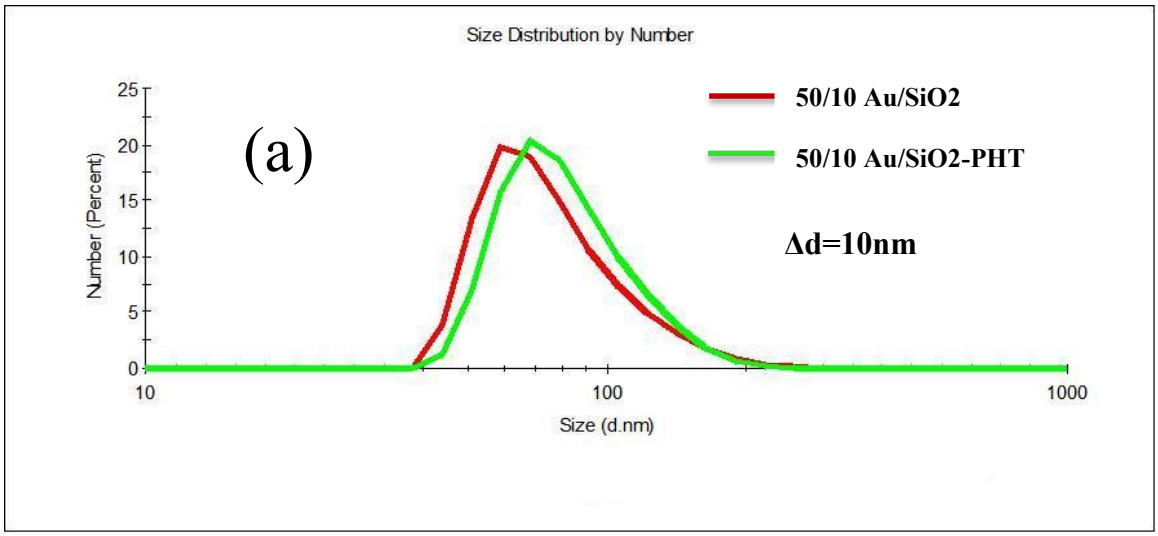
Size Distribution by Number
(a)
50/10 Au/SiO2
50/10 Au/SiO2-PHT
Δd=10nm
Number (Percent)
Size (d.nm)
0
5
10
15
20
25
10
100
1000

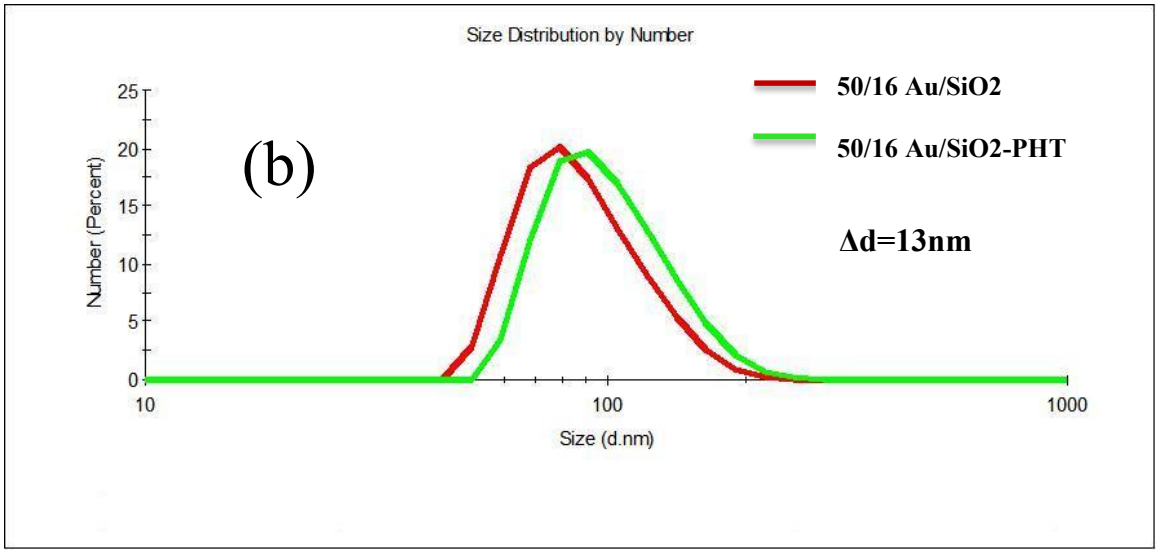
Size Distribution by Number
(b)
50/16 Au/SiO2
50/16 Au/SiO2-PHT
Δd=13nm
Number (Percent)
Size (d.nm)
0
5
10
15
20
25
10
100
1000

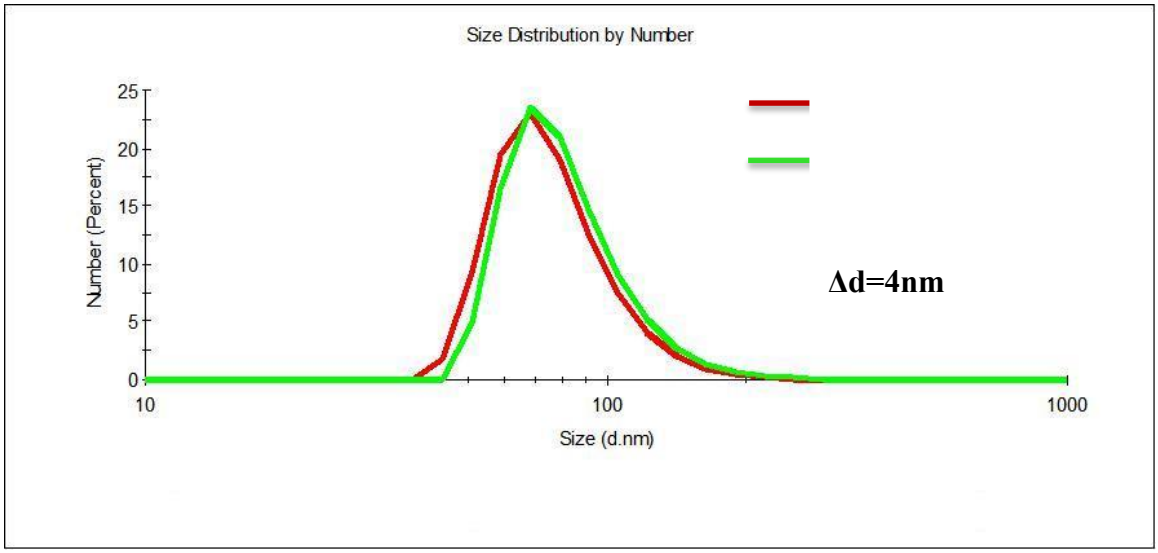

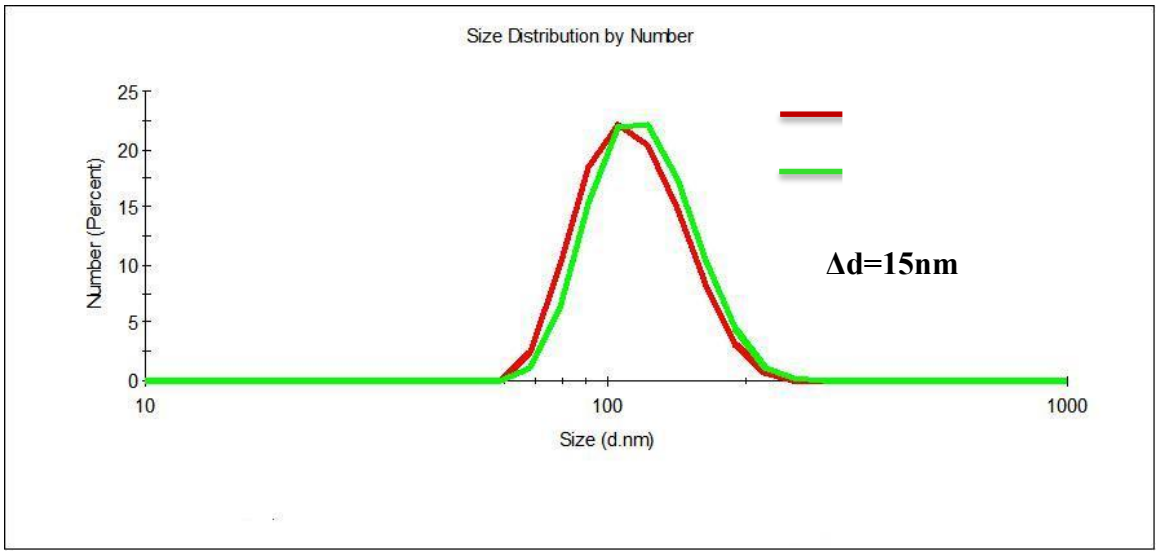

Figure 3. 2: Dynamic light scattering of Au/SiO2 and Au/SiO2-PHT composites. (a) shell thisckness: 10nm. (b) shell thisckness: 16nm. (c) shell thisckness: 19nm. (d) shell thisckness: 30nm.

3.3 Single particle imaging of Au/SiO2-PHT nanocomposites

Fig 3.3 shows (a) the backscattering image recorded with 532nm excitation, and (b) and (c) the fluorescence lifetime images (FLIM) recorded with 440nm and 532nm excitation from the same area of 15x15 microns containing isolated 50nm-core/19nm-shell Au/SiO_2-PHT particles spin coated on a transparent glass substrate. As shown for the particles surrounded by cycles, we can successfully image PHT photoluminescence and scattering of gold from the same nanoparticle using 532nm excitation to confirm again assembly of polymer PHT on the surface of silica shell and formation of Au/SiO_2-PHT nanocomposites. Fig 3.4 shows the lifetime distribution based on the FLIM images (shown Fig 3.3 (b) and (c)), which applys a multiexponential fit to the image on a pixel-by-pixel basis. So the lifetime of so many occurences from the image pixel-by-pixel can be revealed in this distribution. We found lifetime distribution by excitation 532nm is almost same with excitation 440nm. This can be explained that radiative decay rate is almost non-changed in plasmonic effect, which causes unchanged lifetime of PHT.

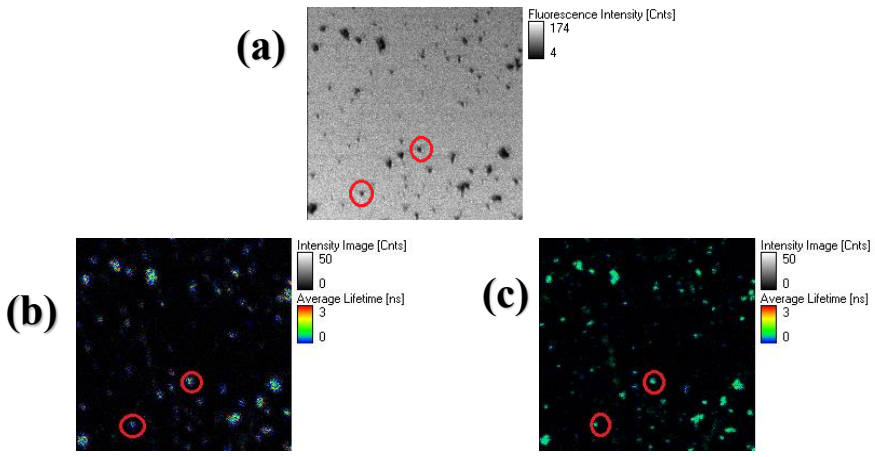

Figure 3. 3: Confocal single particle microscopy of 50nm-core/19nm-shell Au/SiO2-PHT nanocomposites. spin coated on transparent cover glass substrate. Imamge area is 15x15 microns. (a) backscattering image visualizing gold core, (b) FLIM image upon 440nm excitation, and (c) FLIM image upon 532nm excitation.

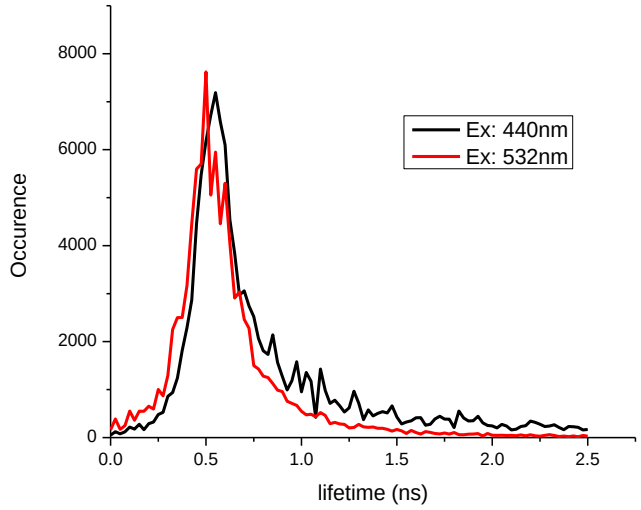

Figure 3. 4: Lifetime distribution of Au/SiO2-PHT by excitation 532nm (red line) and excitation 440nm (black line).

3.4 Dependencies of PL enhancement factor on the SiO2 shell thickness

As discussed before, four types of core/shell Au/SiO2-PHT nanoclusters were subjected to 440 nm (off SPR) and 532nm (at SPR) laser excitation and confocal FLIM investigation. From the FLIM images as those shown in Fig.3.3 we could determine the PL intensity measured with alternate laser excitation and calculate for each nanoparticle the observed PL enhancement for PHT due to the presence of AuNP. Fig 3.5 shows the distribution of the PL enhancement factor estimated from 25 individual 50nm/19nm core/shell Au/SiO2-PHT nanoclusters from FLIM images with alternate laser excitation, calculated according to

$$E_{PL} = (I_{PL}\ (532\ nm)/I_{PL}\ (440\ nm))/\ (Abs\ (532\ nm)/Abs\ (440\ nm) \qquad (3.1)$$

A fit by a Gaussian function estimates a mean value and the width of the distribution from Fig. 3.5 to be 4.6 and 2.31 for the observed PL enhancement for the particular shell of 19nm

Fig.3.6 shows the mean values for the PL enhancement factor obtained for all nanoclusters using similar distributions measured from each 25 nanoclusters of a given type. All nanoclusters show PL enhancement, except for Au/SiO2-PHT nanoclusters with 10nm shell thickness for which we obtained a value close to 1, meaning no enhancement. The highest enhancement is observed for 16nm and 19 nm shell thicknesses, around 4.5 and 4.6nm, and lower for 30nm thickness (about 2nm). These distances are in similar range with the calculations from Fig.1.2 which suggested predicted enhancement at values larger than 15nm separation distance between an emitting molecule with a PL peak at 605nm and a large gold nanoparticle. Since in our case the PL peak of the polymer (580nm) is red shifted from the gold SPR (537-543nm), according to the theoretical treatment of the plasmon-exciton interaction we only expect that the interaction between PHT and AuNP is dominated by energy transfer from the polymer to metal nanoparticle and PL enhancement of the excitation rate and these processes compete to each other. For 10nm shell thickness it seems that the two processes equal in strength or in other words they cancel each other. For larger separation distances (thicker shells), the PL enhancement by the excitation rate overcomes the quenching by energy transfer to the metal nanoparticle and we observe PL enhancement larger than 1, highest at 15nm separation and going down at larger distance, for example at 30nm.

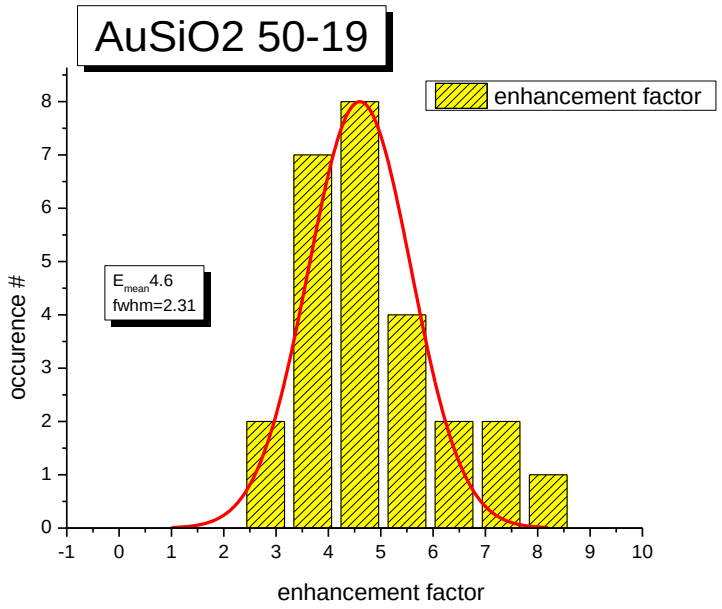

Figure 3. 5: Distribution of the PL enhancement factor from 25 individual 50nm/19nm core/shell Au/SiO2-PHT nanoclusters investigated with alternate 440/532nm laser with the PL detected around 580nm. Also shown is a Gauss fit with a mean value of 4.6 and full width at the half maximum (fwhm) of 2.31.

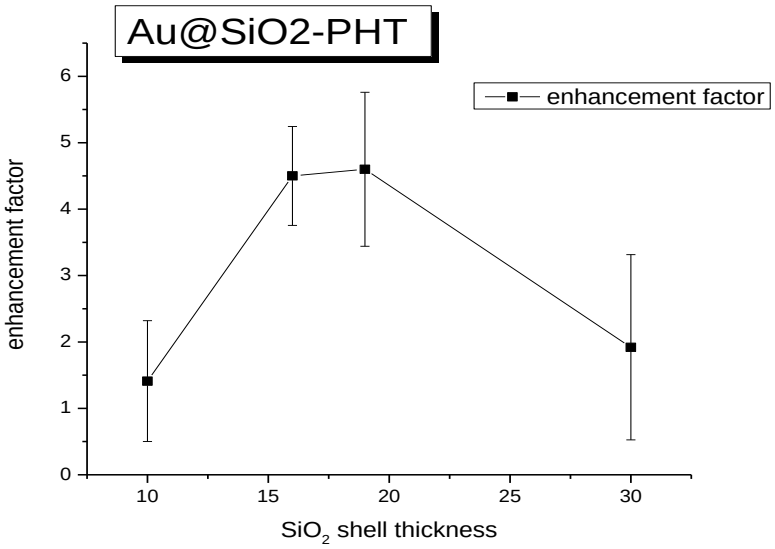

Figure 3. 6: Mean PL enhancement factor for four types of Au/SiO2-PHT.

3.5 Dependencies of PL lifetime on SiO_2 shell thickness

We used pulsed laser excitation and TCSPC detection and this allowed us to estimate PL lifetimes as a function of polymer PHT-AuNP separation distance off and at SPR. Figs. 3.7 and 3.8 show the distribution for PL lifetimes from 25 individual 50nm/19nm core/shell Au/SiO2-PHT nanocomposites obtained by 440nm and 532nm excitation, respectively. Each data point is the result of a fit with a single exponential model and the resulting histogram was fit by a Gauss function, resulting in mean values $P_{mean\ (e)}$ (440nm) = 0.81ns and fwhm (440nm) =0.14ns and $P_{mean\ (e)}$ (532nm) = 0.77ns and fwhm (532nm) =0.22ns, indicating that for nanocomposites with observed PL enhancement there is no change in PL lifetime when exciting either at plasmon resonance or outside. This confirms that the PL enhancement is due to excitation rate enhancement which in turn can increase the overall PL intensity at resonance as discussed in the beginning. The dependency of PL lifetimes measured at the two excitation wavelengths for the four types of Au/SiO2-PHT nanocomposites are shown in Fig 3.9. The experiments at 440nm probe only the PL quenching of PHT by the metal nanoparticle with the PL lifetime decreasing with the decrease of shell thickness which indicates stronger quenching by energy transfer. At 30nm shell thickness, supposedly there is no energy transfer from PHT to metal surface because the distance is too large and the observed PL lifetime is the same as from PHT films alone. At shorter distances (shell thicknesses) we observe increase quenching since the PL lifetime decrease considerably, down to 0.5 ns at 10nm separation. When the nanocomposites are excited at 532nm, the PL lifetime vs. shell thickness is similar in trend with the dependency at 440nm, suggesting that we only obtain PL enhancement by increased excitation rate leading to increased PL quantum yield, as proposed before.

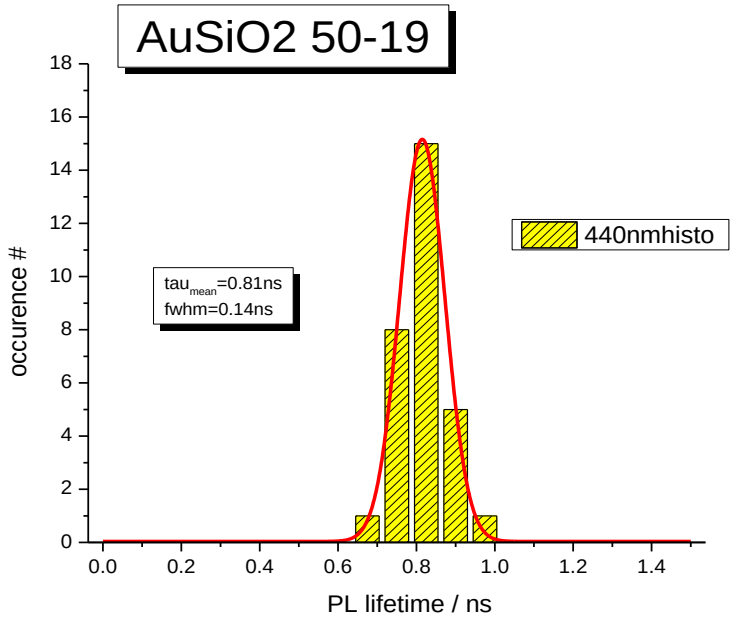

Figure 3. 7: Distribution of PL lifetimes from 25 individual 50nm/19nm core/shell Au/SiO2-PHT measured upon excitation at 440nm. Also shown is a Gauss fit.

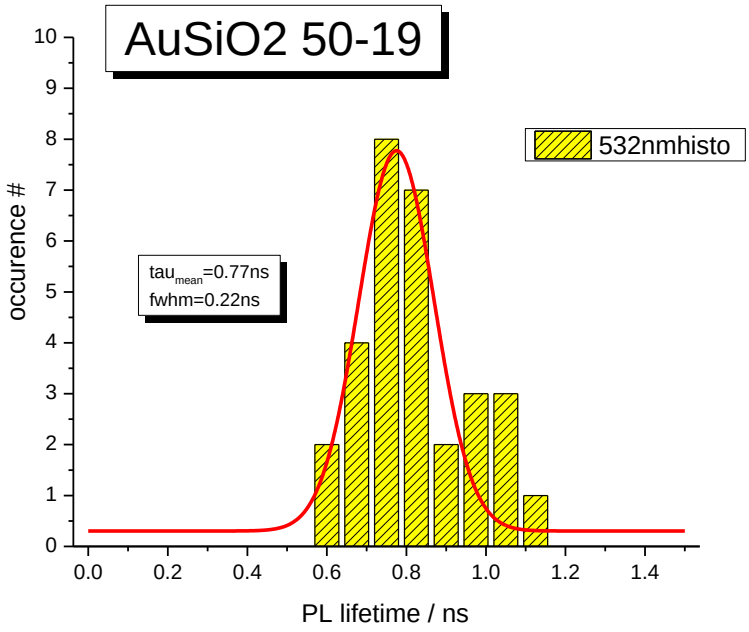

Figure 3. 8: Distribution of PL lifetimes from 25 individual 50nm/19nm core/shell Au/SiO2-PHT measured upon excitation at 532nm. Also shown is a Gauss fit.

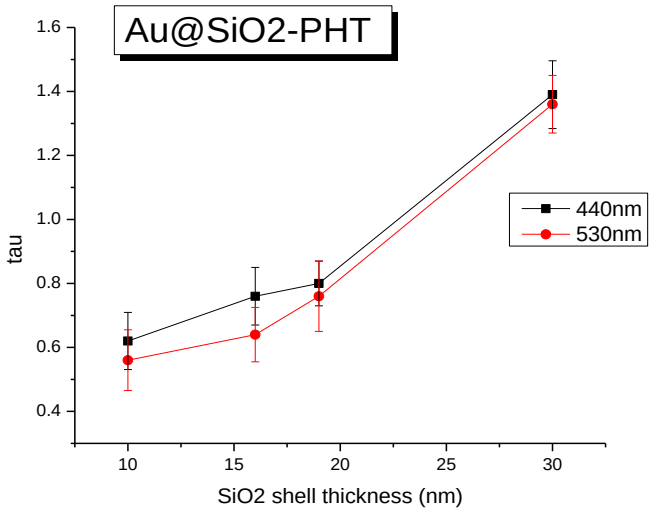

Figure 3. 9: PL lifetime vs Silica shell thickness for Au/SiO2-PHT nanocomposites measured with 532nm (red line) and 440nm (black line) excitation.

3.6 Photoinduced charge transfer from PHT to Cytochrome C in the presence of Au nanoparticles

Cytochrome C is an efficient quencher for PHT fluorescence as it can be seen in Fig 3.10 where PHT photoluminescence is measured at various concentrations of protein, and with increased concentration the PL decay becomes more quenched. Because PHT is a p-type material donating electrons and Cyt-C is known as electron acceptor, quenching of photoexcited PHT by Cyt-C happens most probably by photoinduced electron transfer with the donor and acceptor molecules oppositely charged and binding to each other. To investigate if plasmonic effects can bias the electron transfer between PHT and Cyt-C we conjugated by electrostatic binding Au/SiO2-PHT nanocomposites of 19nm shell thickness and performed FLIM with the two excitations, off SPR at 440nm and at SPR at 532nm. Fig 3.11 shows the distributions of PL intensity measured from Au/SiO2-PHT and Au/SiO2-PHT-CytC nanocomposites with 440nm and 532nm excitation, each distribution containing data from 25 isolated nanocomposites. Using the relationship which defines the quenching efficiency for electron transfer as $E = 1 - {I_{donor-acceptor}}/{I_{donor}}$ with I_{donor} and $I_{donor-acceptor}$ the mean values for the PL intensity obtained form Fig.3.11 by Gauss fits for AuSiO2-PHT as donor and AuSiO2-PHT –CytC as donor-acceptor systems, we estimated efficiencies E(440nm)=63% and E(532nm)=34% which suggests a decrease in electron transfer efficiency when exciting at plasmon resonance. Since we suspect that there might be differences in the loading of PHT between donor and donor-acceptor samples, we also estimated the PL lifetimes of the two sets of samples as this property is not affected by concentration, as opposed to PL intensity. Fig 3.12 shows the distributions of PL lifetimes for Au/SiO2-PHT-Cyt C measured by 440nm and 532nm, each from 25 nanocomposites, with similar mean values around 0.35ns, suggesting there is no effect of the plasmon resonance on the electron transfer rate. Since there is PL enhancement in intensity when the excitation happens at plasmon resonance, up to 4.3 times for this particular sample, it means that

more excitons can be produced and separated in charges when exciting at resonance compared to off-resonance. In other words, even if the rate does not change, the amount of charges per time unit (electrons in Cyt-C and holes in PHT) is larger when exciting at plasmon resonance. Comparing data from Fig.3.12 and 3.7 and 3.8, and using the relation

$$k_{ET} = \frac{1}{\tau_{PHT/Cyt\,C}} - \frac{1}{\tau_{PHT}} \qquad (3.1)$$

We obtain a rate for electron transfer from PHT to CytC of $1.69 \times 10^{9} sec^{-1}$.

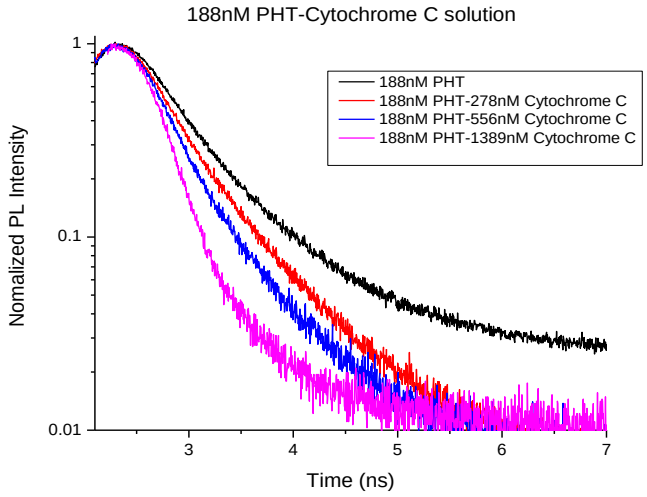

Figure 3. 10: Fluorescence decay (lifetime fluorescence) of polymer PHT solutions with different concentration Cytochrome C.

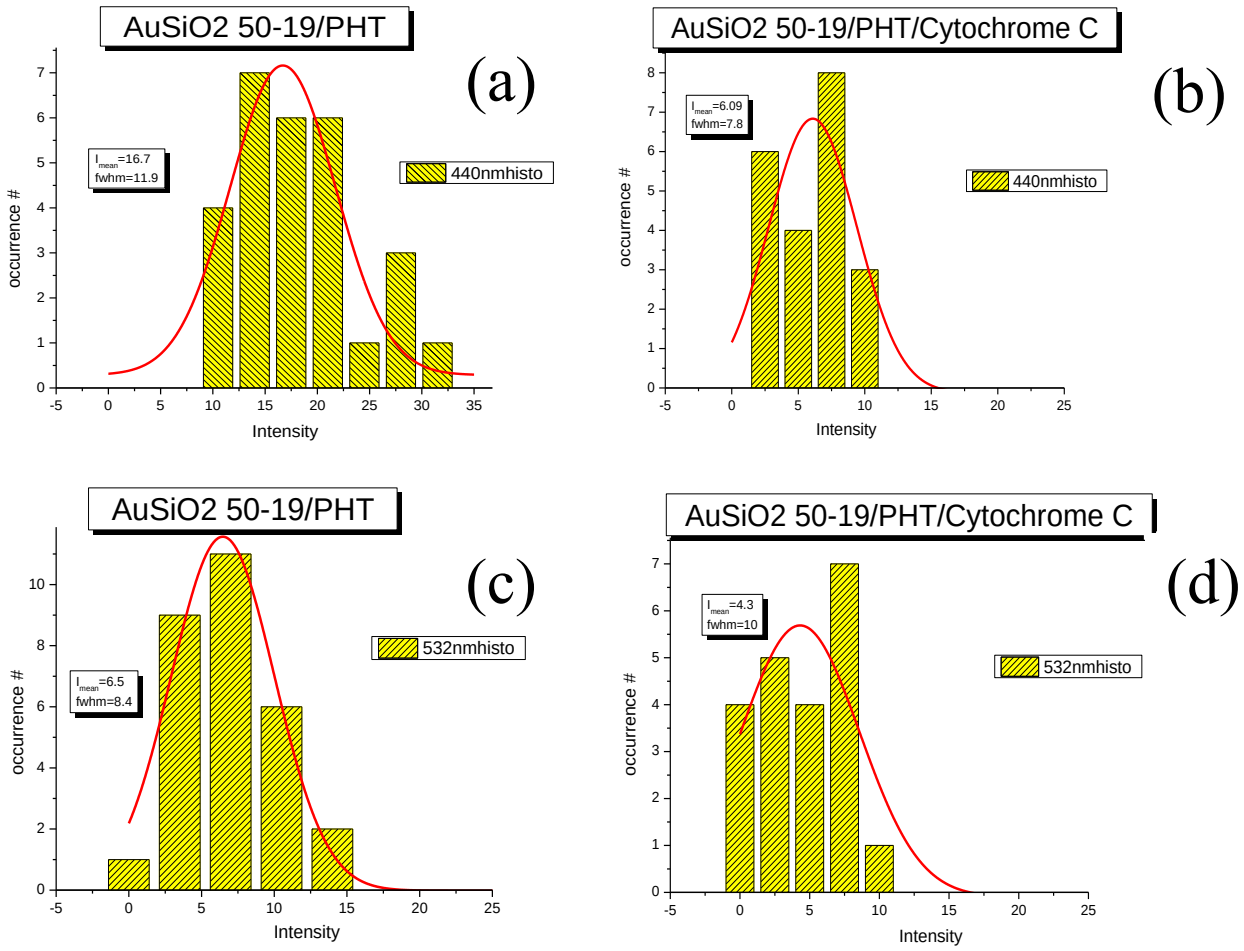

Figure 3. 11: Distribution of PL intensity measured for (a) Au/SiO2-PHT excited at 440nm, (b) Au/SiO2-PHT-Cyt C excited at 440nm, (c) Au/SiO2-PHT excited at 532nm, (d) Au/SiO2-PHT-Cyt C excited at 532nm together with corresponding Gauss fits.

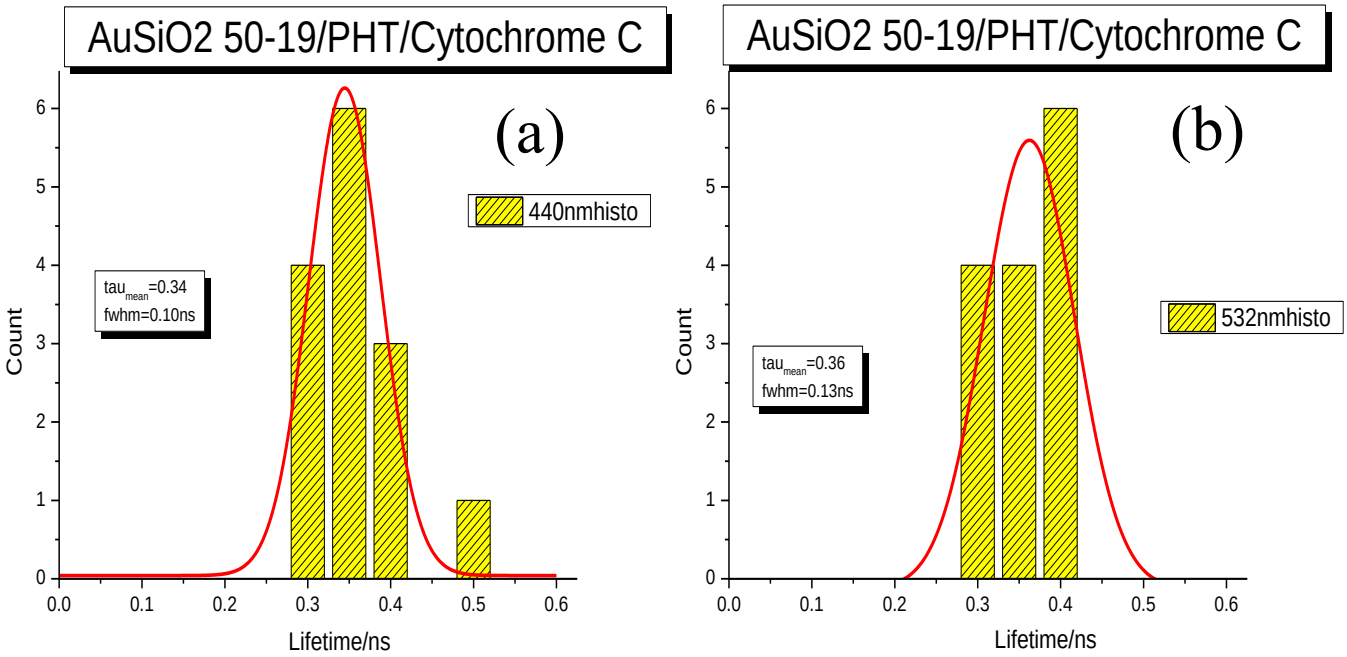

Figure 3. 12: PL lifetime distribution for individual Au/SiO2-PHT-Cytochrome C. (a) 440nm excitation, (b) 532nm excitation. It was fitted by a Gaussian function.

CHAPTER 4. Conclusions

In the present research report we designed self-assembled and optically characterized a series of plasmonic nanoclusters based on core/shell gold nanoparticle/silica scaffolds capped with a conjugated polymer (PHT) with optical output, here photoluminescence, tunable by the variation of the silica shell thickness. Using dynamic light scattering and a combination of confocal backscattering and photoluminescence microscopy with single particle sensitivity we demonstrated formation of Au/SiO2-PHT composites particle and non-aggregation in solution. By varying the size of the thickness of the silica shell (10nm, 16nm, 19nm and 30nm), we could produce plasmonic nanoclusters with controlled optical (PL) output, from efficient PL quenching to PL enhancement. Single molecule microscopy (SMS) by alternate two color excitation was used to characterize the optical properties of the nanoclusters and to understand the mechanism of interaction between plasmon (AuNP) and exciton (PHT). Experiments at 440nm excitation characterized the photoluminescence quenching by energy transfer to the metal nanoparticle while those at 532nm demonstrated enhancement in polymer photoluminescence due to an increase in optical excitation rate as a result of local electric field enhancement produced by the presence of Au nanoparticle. The highest enhancement was observed for nanocomposites with a shell thickness around 15-19 nm, of about 4 times when excited at plasmon resonance. Finally, we tested the utilization of these nanoclusters in combination with an electron acceptor moiety, cytochrome c to find that indeed the Au nanoparticle does not modify the rate for electron transfer between PHT and CytC but it does increase the amount of charges that can be extracted from such donor-acceptor per time unit by creating more excitons at plasmon resonance then off resonance.

BIBLIOGRAPHY

[1] Brongersma M. L. & Kik P. G. Surface Plasmon Nanophotonics (Springer, Dordrecht, 2007).

[2] Zeng, S.; Yong, Ken-Tye; Roy, Indrajit; Dinh, Xuan-Quyen; Yu, Xia; Luan, Feng (2011). "A review on functionalized gold nanoparticles for biosensing applications". Plasmonics 6 (3): 491–506.

[3] Maier S. A. et al. Local detection of electromagnetic energy transport below the diffraction limit in metal nanoparticle plasmon waveguides. Nature Mat 2, 229–232 (2003)

[4] Daniel, M. C., Astruc, D. Gold nanoparticles: Assembly, supramolecular chemistry, quantum-size-related properties, and applications toward biology, catalysis, and nanotechnology. Chemical Review. 2004, 104, pp. 293-346.

[5] J. I. L. Chen, Y. Chen, and D. S. Ginger, "Plasmonic nanoparticle dimers for optical sensing of DNA in complex media," J. Am. Chem. Soc. 132, 9600–9601 (2010).

[6] A. D. Rakic, A. B. Djurišic, J. M. Elazar, and M. L. Majewski, "Optical properties of metallic films for vertical—cavity optoelectronic devices," Appl. Opt. 37, 5271–5283 (1998).

[7] "Plasmonic nanoparticle enhanced light absorption in GaAs solar cells," K. Nakayama, K Tanabe, and H. A. Atwater, Appl. Phys. Lett. 93, 121904 (2008).

[8] Lu Y and Chen X. Plasmon-enhanced luminescence in Yb3+: Y2 O3 thin film and the potential for solar cell photon harvesting. Appl. Phys. Lett. 2009; 94: 193110-2.

[9] P. S. Daniel †, Lee A. Jointly Tuned Plasmonic–Excitonic Photovoltaics Using Nanoshells. Nano Lett. (2013); DOI: 10.1021/nl304604y.

[10] Chaki, N.K., Vijayamohanan, K., 2002, Self-assembled monolayers as a tunable platform for biosensor applications, Biosensors and Bioelectronics, 17, 1-12.

[11] B. R. Eggins, Chemical Sensors and Biosensors (Analytical Techniques in the Sciences), John Wiley & Sons Ltd, Chichester, UK, 2002.

[12] Hartling, Optics Express 2007, vol 15 no 20 page 12806

[13] K. B. Crozier, A. Sundaramurthy, G. S. Kino, and C. F. Quate, "Optical antennas: resonators for local field enhancement," J. Appl. Phys. 94, 4632-4642 (2003).

[14] Lei Zhao, Journal of Physical Chemistry C, 2012, 116, 8287

[15] P. Anger, P. Bharadwaj, and L. Novotny, "Enhancement and quenching of single molecule fluorescence," Phys. Rev. Lett. 96(11), 113002 (2006).

[16] Y. Wang, T. Yang, M. T. Tuominen, and M. Achermann, "Radiative rate enhancements in ensembles of hybrid metal-semiconductor nanostructures," Phys. Rev. Lett. 102(16), 163001 (2009).

[17] Jensen, T. R.; Malinsky, M. D.; Haynes, C. L.; Van Duyne, R. P. (2000) "Nanosphere

Lithography: Tunable Localized Surface Plasmon Resonance Spectra of Silver Nanoparticles" J.Phys. Chem. B 104 (45), 10549–10556.

[18] Link, S. & El-Sayed, M. A. Spectral properties and relaxation dynamics of surface plasmon electronic oscillations in gold and silver nanodots and nanorods. J. Phys.

Chem. B 103, 8410–8426 (1999).

[19] Kreibig U and Vollmer M 1995 Optical Properties of Metal Clusters (Springer Series in Materials Science vol 25) (Berlin: Springer) and references therein)

[20] Kummerlen, J.; Leitner, A.; Brunner, H.; Aussenegg, F. R.; Wokaun, A.; (1993) "Enhanced dye fluorescence over silver island films: Analysis of the distance dependence".Mol. Phys. 80 (5), 1031–1046.

[21] Anger, Novotny PRL 2006, 96, 113002.

[22] Lakowicz, J. R.; Shen Y, D'Auria, S.; Malicka J.; Fang J.; Gryczynski Z.; and Gryczynski I.; (2002) "Radiative decay engineering: Effects of Silver Island Films on Fluorescence Intensity, Lifetimes, and Resonance Energy Transfer"Anal. Biochem. 301, 261-277.

[23] M. M. Maye, O. Gang and M. Cotlet. Photoluminescence enhancement in CdSe/ZnS–DNA linked–Au nanoparticle heterodimers probed by single molecule spectroscopy. Chem. Commun.46, 6111-6113 (2010).

[24] Zhang, S. Fabrication of novel biomaterials through molecular self-assembly. Nat. Biotech. 2003, 21, 1171–1178.

[25] Claessens, C.G.; Stoddart, J.F. π–π interactions in self-assembly. J. Phys. Org. Chem. 1997, 10, 254–272.

[26] Sherrington, D.C.; Taskinen, K.A. Self-assembly in synthetic macromolecular systems multiple hydrogen bonding interactions. Chem. Soc. Rev. 2001, 30, 83–93.

[27] Ozin and Arsenault (2005). Nanochemistry: a chemical approach to nanomaterials. Cambridge: Royal Society of Chemistry.

[28] Li HY, Carter JD, LaBean TH. Nanofabrication by DNA Self-Assembly. Materials Today. 2009; 12:20–28.

[29] Alivisatos, 2003 The use of nanocrystals in biological detection. Nature Biotechnology 22 4752.

[30] Ariga, K.; Hill, J. P.; Ji, Q. M.Layer-by-Layer Assembly as a Versatile Bottom-up Nanofabrication Technique for Exploratory Research and Realistic Application Phys. Chem. Chem. Phys. 2007, 9, 2319– 2340[CrossRef], [PubMed], [CAS].

[31] M. T. Zin, H. Ma, A. M. Munro, D. S. Ginger, M. Gungormus, K. Leong, C. Tamerler, M. Sarikaya and A. K.-Y. Jen, "Well-Controlled Arrays of Core-Shell Quantum Dots with Tunable Photoluminescence Properties", Poly. Mater. Sci. Eng., 95 1002-1003 (2006).

[32] H. R. Wang, Y. J. Song, Z. C.Wang, C. J. Medforth, J. E. Miller, L. Evans, P. Li, and J. A. Shelnutt. Silica-Metal Core-Shells and Metal Shells Synthesized by Porphyrin-Assisted Photocatalysis. Chem. Mater. 2008, 20: 7434–7439

[33] P. Schurtenberger, and M. Newman, "Characterization of Biological and Environmental Particles using Static and Dynamic Light Scattering", In Environmental Particles, J. Buffle, H. van Leeuwen, Eds.; Lewis Publishers: Boca Raton, 1993, 37-115.

[34] B. J. Berne and R. Pecora, Dynamic Light Scattering, Dover Publications, Mineola (2000).

[35] BERNE, B.J. AND PECORA, R. (2000). DynamicLight Scattering with Applications to Biology, Chemistry, and Physics. Mineola, NY: Dover Publications

[36] Xie, X. S., Choi, P. J., Li, G. W., Lee, N. K. and Lia, G. Single-molecule approach to molecular biology in living bacterial cells. Annual Review of Biophysics 37: 417-444 (2008).

[37] Walter, N. G. Future of biomedical sciences: Single molecule microscopy. Biopolymers 85: 103-105 (2007).

[38] R. Cubeddu, D. Comelli, C. D'Andrea, P. Taroni, and G. Valentini. Time-resolved fluorescence imaging in biology and medicine. Journal of Physics D-Applied Physics, 35(9):R61–R76, 2002.

[39] M. Kollner and J. Wolfrum. How many photons are necessary for fluorescence-lifetime measurements? Chemical Physics Letters, 200(1-2):199–204, 1992.

[40] Xu, Z. and Cotlet, M. (2011), Quantum Dot–Bridge–Fullerene Heterodimers with Controlled Photoinduced Electron Transfer. Angew. Chem. Int. Ed., 50: 6079–6083. doi: 10.1002/anie.201007270

[41] Seidel C.A.M. Single Molecule 2, 251 (2001).